Description of quadrupole collectivity in $N \approx 20$ nuclei with techniques beyond the mean field

R. R. Rodríguez-Guzmán, J. L. Egido, and L. M. Robledo
Departamento de Física Teórica C-XI, Universidad Autónoma de Madrid, E-28049-Madrid, Spain
(Received 9 June 2000; published 23 October 2000)

Properties of the ground and several collective excited states of the light nuclei ^{30,32,34}Mg are described in the framework of the angular momentum projected generator coordinate method using the quadrupole moment as collective coordinate and the Gogny force as the effective interaction. The calculated excitation energies and $B(E2)$ transition probabilities agree reasonably well with experiment. The results clearly indicate that both the restoration of the rotational symmetry and the quadrupole dynamics are key ingredients for the description of the properties of the above-mentioned nuclei.

PACS number(s): 21.60.Jz, 21.10.Re, 21.10.Ky, 27.30.+t

I. INTRODUCTION

Nowadays, the region of neutron-rich nuclei around $N=20$ is the subject of active research both in the experimental and theoretical side. The reason is the strong experimental evidence towards the existence of quadrupole deformed ground states in this region. The existence of deformed ground states implies that $N=20$ is not a magic number for the nuclei considered, opening up the possibility for a better understanding of the mechanisms behind the shell structure in atomic nuclei. In addition, the extra binding energy coming from deformation can help to extend thereby the neutron drip line in this region far beyond what could be expected from spherical ground states. Among the variety of available experimental data, the most convincing evidence for a deformed ground state is found in the ^{32}Mg nucleus where both the excitation energy of the lowest lying 2^+ state [1] and the $B(E2,0^+ \rightarrow 2^+)$ transition probability [2] have been measured. Both quantities are fairly compatible with the expectations for a rotational state. Theoretically, from a shell-model point of view, the deformed ground states are a consequence of the lower energies of some intruder $2p-2h$ neutron excitations into the fp shell as compared to the pure sd configuration [3]. In terms of the mean-field picture of the nucleus, a quadrupole deformed ground state only appears after taking into account the zero-point rotational energy correction to the mean-field energy [4–8].

In a previous paper [9] we have computed angular momentum projected (AMP) energy landscapes, as a function of the mass quadrupole moment, for the nuclei $^{30-34}$Mg and $^{32-38}$Si. We have found that the projection substantially changes the conclusions extracted from a pure mean-field calculation. In all the nuclei considered, with the exception of ^{34}Mg, two coexistent configurations (prolate and oblate) have been found with comparable energy indicating thereby that configuration mixing of states with different quadrupole intrinsic deformation had to be considered. The purpose of this paper is to study the effect of such configuration mixing for the nuclei $^{30-34}$Mg. The Si isotopes have been disregarded in this work as there are indications [7] that triaxiality effects could be relevant for the description of their ground states and, for the moment, our calculations are restricted to axially symmetric ($K=0$) configurations. In our calculations we have used the Gogny force [10] (with the D1S parametrization [11]) which is known to provide reasonable results for many nuclear properties such as ground-state deformations, moments of inertia, fission barrier parameters, etc., all over the periodic table. As the results presented in this paper will show, this force is also suited for the description of quadrupole collectivity in $N \approx 20$ nuclei. Additional results for ^{32}Mg with older parametrizations of the Gogny force are also discussed. Finally, let us mention that similar calculations to the ones discussed here using the Skyrme interaction have recently been reported [12].

II. THEORETICAL FRAMEWORK

To compute the properties of the ground and several collective excited states of the nuclei considered in this paper we have used the angular momentum projected generator coordinate method (AMP-GCM) with the mass quadrupole moment as generating coordinate. To this end, we have used the following ansatz for the $K=0$ wave functions of the system:

$$|\Phi^I_\sigma\rangle = \int dq_{20} f^I_\sigma(q_{20}) \hat{P}^I_{00} |\varphi(q_{20})\rangle. \tag{1}$$

In this expression $|\varphi(q_{20})\rangle$ is the set of axially symmetric (i.e., $K=0$) Hartree-Fock-Bogoliubov (HFB) wave functions generated by constraining the mass quadrupole moment to the desired values $q_{20}=\langle\varphi(q_{20})|z^2-1/2(x^2+y^2)|\varphi(q_{20})\rangle$ (please, notice that this definition is a factor of 1/2 smaller than the usual definition of the intrinsic quadrupole moment). The intrinsic wave functions $|\varphi(q_{20})\rangle$ have been expanded in a harmonic oscillator (HO) basis containing ten major shells and with equal oscillator lengths to make the basis closed under rotations [13]. The rotation operator in the HO basis has been computed using the formulas of [14].

The operator

$$\hat{P}^I_{00} = \frac{2I+1}{8\pi^2} \int d\Omega d^I_{00}(\beta) e^{-i\alpha \hat{J}_z} e^{-i\beta \hat{J}_y} e^{-i\gamma \hat{J}_z} \tag{2}$$

is the usual angular momentum projector with the $K=0$ restriction [15] and $f^I_\sigma(q_{20})$ are the ''collective wave functions'' solution of the Hill-Wheeler (HW) equation

$$\int dq'_{20}\mathcal{H}^I(q_{20},q'_{20})f^I_\sigma(q'_{20}) = E^I_\sigma \int dq'_{20}\mathcal{N}^I(q_{20},q'_{20})f^I_\sigma(q'_{20}). \quad (3)$$

In the equation above we have introduced the projected norm $\mathcal{N}^I(q_{20},q'_{20})=\langle\varphi(q_{20})|\hat{P}^I_{00}|\varphi(q'_{20})\rangle$, and the projected Hamiltonian kernel $\mathcal{H}^I(q_{20},q'_{20})=\langle\varphi(q_{20})|\hat{H}\hat{P}^I_{00}|\varphi(q'_{20})\rangle$. As the generating states $\hat{P}^I_{00}|\varphi(q_{20})\rangle$ are not orthogonal, the ''collective amplitudes'' $f^I_\sigma(q_{20})$ cannot be easily interpreted. This drawback can be easily overcome by introducing [16] the so-called ''natural'' states

$$|k^I\rangle=(n^I_k)^{-1/2}\int dq_{20}u^I_k(q_{20})\hat{P}^I_{00}|\varphi(q_{20})\rangle,$$

which are defined in terms of the eigenstates $u^I_k(q_{20})$ and eigenvalues n^I_k of the projected norm, i.e., $\int dq'_{20}\mathcal{N}^I(q_{20},q'_{20})u^I_k(q'_{20})=n^I_k u^I_k(q_{20})$. The correlated wave functions $|\Phi^I_\sigma\rangle$ are written in terms of the natural states as

$$|\Phi^I_\sigma\rangle=\sum_k g^{\sigma,I}_k|k^I\rangle,$$

where the new amplitudes $g^{\sigma,I}_k$ have been introduced. In terms of the amplitudes $g^{\sigma,I}_k$ the collective wave functions

$$g^I_\sigma(q_{20})=\sum_k g^{\sigma,I}_k u^I_k(q_{20}) \quad (4)$$

are defined. They are orthogonal and therefore their module squared has the meaning of a probability. The introduction of the natural states also reveals a particularity of the HW equation: if the norm has eigenvalues with zero value they have to be removed for a proper definition of the natural states (i.e., linearly dependent states are removed from the basis). In practical cases, in addition to the zero value eigenvalues also the eigenvalues smaller than a given threshold have to be removed to ensure the numerical stability of the solutions of the HW equation. In order to account for the fact that the mean value of the number of particles operator $\langle\Phi^I_\sigma|\hat{N}_\tau|\Phi^I_\sigma\rangle$ ($\tau=\pi,\nu$) usually differs from the nucleus' proton and neutron numbers, we have followed the usual recipe [17,18] of replacing the Hamiltonian by $\hat{H}-\lambda_\pi(\hat{N}_\pi-Z)-\lambda_\nu(\hat{N}_\nu-N)$, where λ_π and λ_ν are chemical potentials for protons and neutrons, respectively.

Concerning the density-dependent part of the Gogny force we have use the usual prescription already discussed in Refs. [18,9,19]. It amounts to using the density

$$\rho(\vec{r})=\frac{\langle\varphi(q_{20})|\hat{\rho}e^{-i\beta\hat{J}_y}|\varphi(q'_{20})\rangle}{\langle\varphi(q_{20})|e^{-i\beta\hat{J}_y}|\varphi(q'_{20})\rangle} \quad (5)$$

in the density-dependent part of the interaction when the evaluation of $\langle\varphi(q_{20})|\hat{H}e^{-i\beta\hat{J}_y}|\varphi(q'_{20})\rangle$ is required in the calculation of the projected Hamiltonian kernels.

It has to be kept in mind that the solution of the HW equation for each value of the angular momentum I determines not only the ground state ($\sigma=1$), which corresponds to the yrast band, but also excited states ($\sigma=2,3,\ldots$) that, with the set of generating wave functions used in these calculations, could correspond to solutions with a different deformation from the one of the ground state and/or to quadrupole vibrational bands.

Finally, let us mention that, as the intrinsic wave functions $|\varphi(q_{20})\rangle$ are determined before the projection onto angular momentum, the procedure described above is of the ''projection after variation'' (PAV) type. It is well known [16] that the PAV method yields the wrong moments of inertia, at least in the translational case, and a way to cure this deficiency is to consider a ''projection before variation'' (PBV) which is much more difficult to implement because the intrinsic wave functions have to be determined for each value of the angular momentum I using the Ritz variational principle on the projected energy (see [20] for the application of PBV with small configuration spaces). To illustrate the consequences of the PBV method it is convenient to consider a strongly deformed intrinsic configuration $|\varphi(q_{20})\rangle$, as in this case it is possible to obtain [16] an approximate expression for the (PAV) projected energy

$$E_{PAV}(I)=\langle H\rangle-\frac{\langle\vec{J}^2\rangle}{2\mathcal{J}_Y}+\frac{\hbar^2 I(I+1)}{2\mathcal{J}_Y},$$

where $\mathcal{J}_Y$ is the Yoccoz (Y) moment of inertia. In this expression we recognize the rotational energy correction $\langle\vec{J}^2\rangle/2\mathcal{J}_Y$ and the usual rotorlike expression for the energy of the band $\hbar^2 I(I+1)/2\mathcal{J}_Y$. It was shown in [21] (see also [22]) that starting from the projected energy and making an approximate projection before variation (PBV) one obtains for the energy of the rotational band the following expression:

$$E_{PBV}(I)=\langle H\rangle-\frac{\langle\vec{J}^2\rangle}{2\mathcal{J}_Y}+\frac{\hbar^2 I(I+1)}{2\mathcal{J}_{TV}},$$

where $\mathcal{J}_{TV}$ is the Thouless-Valatin moment of inertia. This implies that for the determination of the zero-point rotational energy correction (which is very important as it can dramatically change the energy landscape as a function of the quadrupole moment), one has to use the Yoccoz moment of inertia (i.e., PAV is good) but for the moment of inertia of the band, one has to use the Thouless-Valatin expression or carry out a full PBV calculation.

Taking into account that, in the limit of strong deformation the PBV for the restoration of the rotational symmetry yields to the well-known self-consistent cranking (SCC) method, a possible way to improve the AMP-GCM would be to consider for the intrinsic states a set of wave functions $|\varphi^I(q_{20})\rangle$ as the solution of the SCC-HFB equations for each spin I. However, this would lead to a triaxial projection which is extremely time consuming and also to the issue of how to handle configurations with q_{20} values close to sphericity where the SCC-HFB is no longer a good approximation to the PBV theory.

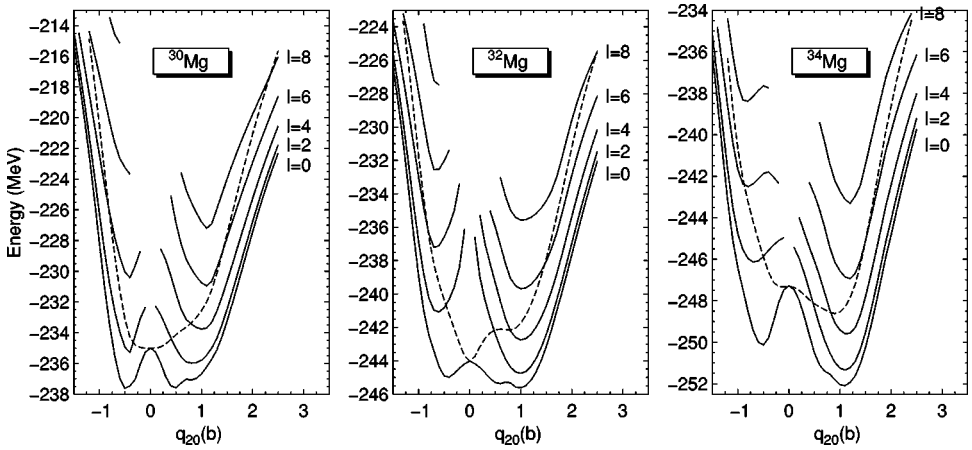

FIG. 1. The HFB (dashed line) and angular momentum-projected energies ($I=0\hbar,2\hbar,\ldots,8\hbar$) for the nuclei considered. See text for further comments.

In order to explore the effect of the PBV in our calculations we will restrict ourselves to performing SCC-HFB calculations for selected configurations and compare the results with those of an AMP calculation on those configurations in order to extract the SCC and Yoccoz moments of inertia. The result of the comparison is that the AMP γ-ray energies are typically a factor of 1.4 bigger than the self-consistent ones and therefore a way to incorporate the effects of PBV would be to quench the bands generated by the AMP-GCM by a factor $1/1.4\approx 0.7$. From a physical point of view it is rather simple to understand why the AMP rotational band energies are higher than the SCC ones. For the sake of simplicity we will concentrate on the 0^+ and 2^+ states. The effect of the PBV on the 0^+ state is to incorporate into the corresponding intrinsic state admixtures of two, four, etc., quasiparticle configurations coupled to $K=0$. For the 2^+ state we can also mix $K=1$ and $K=2$ multiquasiparticle configurations that make the variational space bigger and therefore leads to a higher energy gain for the 2^+ state as compared to the energy gain of the 0^+ state reducing thereby the corresponding 2^+ γ ray energy.

III. DISCUSSION OF THE RESULTS

A. Mean-field and angular momentum-projected energies

In Fig. 1 we have plotted the $I=0\hbar$, $2\hbar$, $4\hbar$, $6\hbar$, and $8\hbar$ projected energies $E^I(q_{20})=\mathcal{H}^I(q_{20},q_{20})/\mathcal{N}^I(q_{20},q_{20})$ as a function of q_{20} for the nuclei ^{30,32,34}Mg. The HFB energies have also been plotted for comparison. The projected energy curves can be regarded as the potential energies felt by the quadrupole collective motion and therefore give us indications of where the collective wave functions will be concentrated.

Before commenting on the physical contents of the curves we have to mention that, except for the $I=0\hbar$ curves, several values around $q_{20}=0$ are omitted. They correspond to intrinsic configurations with a very small value of the norm $\mathcal{N}^I(q_{20},q_{20})$, that is, to configurations whose $I=2\hbar,4\hbar,\ldots$ contents are very small. As a consequence, the evaluation of the projected energies in these cases is vulnerable to strong numerical inaccuracies. Fortunately, the smallness of their projected norms guarantees that these configurations do not play a role in the configuration mixing calculation (the associated norm eigenvalues n_k^I are very small) and therefore can be safely omitted.

Coming back to the projected energy surfaces, we observe that for $I=0\hbar$ and $2\hbar$ a prolate and an oblate minima appear with almost the same energy for the nucleus ^{30}Mg whereas the prolate minimum becomes deeper than the oblate one for ^{32,34}Mg. For increasing spins either the prolate minimum becomes significantly deeper than the oblate one or the oblate minimum is washed out. The prolate minima are located, for all nuclei and spin values, around $q_{20}=1b$ which corresponds to a β deformation parameter of 0.4. On the other hand, the HFB energy curves show a behavior rather different from the $I=0\hbar$ projected curves showing a spherical minimum for ^{30,32}Mg and a prolate one for ^{34}Mg.

To disentangle the relevant configurations of the intrinsic wave functions we have computed their spherical orbit occupancies which are given by

$$\nu(nlj)=\langle\varphi(q_{20})|\sum_m c^+_{nljm}c_{nljm}|\varphi(q_{20})\rangle, \qquad (6)$$

where c_{nljm} are the annihilation operators corresponding to spherical harmonic oscillator wave functions. In the nucleus ^{32}Mg the neutron $\nu(1f_{7/2})$ occupancy is zero for $q_{20}=0$ whereas it is almost 2 at the minimum of the projected energy (i.e., $q_{20}=1b$). The conclusion is clear, the zero-point energy associated with the restoration of the rotational symmetry favors the configuration in which a couple of neutrons have been promoted from the sd shell to the $f_{7/2}$ orbit. This is in good agreement with the shell-model picture of deformation in these nuclei [3].

Through exhaustive mean-field studies of the nucleus ^{32}Mg with several parametrizations of the Skyrme interaction [8] it has become clear that the occurrence of deformation in this nucleus is correlated to the relative position between the $f_{7/2}$ and $d_{3/2}$ neutron orbitals. In our case (D1S parametrization of the Gogny interaction) the so-called $sd-pf$ spherical shell gap for neutrons in the nucleus ^{32}Mg, which is given by $\Delta\epsilon_{f_{7/2}-d_{3/2}}=\epsilon_{f_{7/2}}-\epsilon_{d_{3/2}}$ (with ϵ being the single-particle energies of the spherical configuration), takes the value 5.4 MeV. This value is compatible with the results of [8] and also with the value given in [23]. Furthermore, the $f_{7/2}-p_{3/2}$ spherical energy gap is only 1.8 MeV and there-

fore we expect strong quadrupole correlations between these two orbits. The values for other parametrizations of the Gogny force will be discussed in the last subsection. Finally, let us mention that the quantity $\Delta\epsilon_{f_{7/2}-d_{3/2}}$ is not well defined for the ^{30}Mg and ^{34}Mg nuclei as in these two cases we have appreciable neutron pairing correlations and only the quasiparticle energies are meaningful.

B. Angular momentum-projected generator coordinate calculations

In Fig. 2 the collective wave functions squared $|g^I_\sigma(q_{20})|^2$ [see Eq. (4)] for the two lowest solutions $\sigma=1$ and 2 obtained in the AMP-GCM calculations are depicted. We also show in each panel the projected energy for the corresponding spin. We observe that the 0^+_1 ground-state wave functions of the ^{30}Mg and ^{32}Mg nuclei contain significant admixtures of the prolate and oblate configurations whereas for ^{34}Mg the wave function is almost completely located inside the prolate well. At higher spins, however, the ground-state wave functions are located inside the prolate well in all the nuclei studied. Concerning the first excited states ($\sigma=2$) we notice that in the nucleus ^{34}Mg and for spins higher than zero the collective wave functions show a behavior reminiscent of a β vibrational band: they are located inside the prolate wells and have a node at a q_{20} value near the point where the ground-state collective wave functions attain their maximum values. Contrary to the case of a pure β band, the collective wave functions of Fig. 2 are not symmetric around the node and therefore cannot be considered as harmonic vibrations. On the other hand, the 0^+_2 state of ^{34}Mg is an admixture of prolate and oblate configurations and cannot be considered as a β vibrational state. The same pattern is also seen in the other two nuclei but with slight differences: the β-like bands appear at spins 4 and 6 for ^{32}Mg and ^{30}Mg, respectively.

It is also worth pointing out that from the position of the tails of the collective wave functions relative to the projected energies (see figure caption), we can read the energy gain due to considering the quadrupole fluctuations. The energy gain is maximal at $I=0\hbar$ (0.9, 1, and 0.7 MeV for ^{30}Mg, ^{32}Mg, and ^{34}Mg, respectively) and quickly decreases with increasing spin reflecting the narrowing of the projected wells with spin. The $S(2n)$ separation energies are now 7.8 and 6.13 MeV for ^{32}Mg and ^{34}Mg, respectively, to be compared to the values obtained with the angular momentum projection [9] alone (7.65 and 6.39 MeV) and with the experimental values of 8.056 and 6.896 MeV.

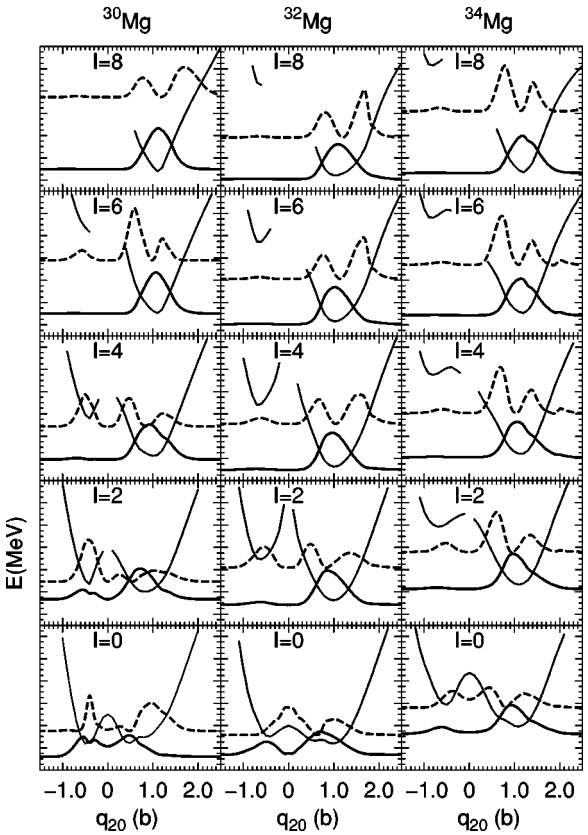

FIG. 2. The collective amplitudes $|g^I_\sigma(q_{20})|^2$ (thick lines) for $\sigma=1$ (full) and 2 (dashed) and spin values of $I=0\hbar,\ldots,8\hbar$ for the nuclei ^{30}Mg, ^{32}Mg, and ^{34}Mg. The projected energy curve for each spin is also plotted (thin line). The *y*-axis scales are in energy units and always span an energy interval of 13 MeV (minor ticks are 0.5 MeV apart). The collective wave functions $|g^I_\sigma(q_{20})|^2$ have also been plotted against the energy scale after a proper scaling and shifting, that is, the quantity $E^I_\sigma+15\times|g^I_\sigma(q_{20})|^2$ is the one actually plotted. With this choice of scales we can read from the figure the energy gain due to the quadrupole fluctuations by considering the position of the wave functions' tail relative to the projected curve.

In order to understand in a more quantitative way the collective wave functions just discussed it is convenient to analyze the quantities

$$(\overline{q}_{20})^I_\sigma=\int dq_{20}|g^I_\sigma(q_{20})|^2 q_{20}, \tag{7}$$

TABLE I. The average intrinsic quadrupole moment $(\overline{q}_{20})^I_\sigma$ and fluctuations $\Sigma^I_\sigma=\sqrt{(\overline{q^2_{20}})^I_\sigma}$ in barns for the three nuclei considered.

	^{30}Mg				^{32}Mg				^{34}Mg			
I	$(\overline{q}_{20})^I_1$	Σ^I_1	$(\overline{q}_{20})^I_2$	Σ^I_2	$(\overline{q}_{20})^I_1$	Σ^I_1	$(\overline{q}_{20})^I_2$	Σ^I_2	$(\overline{q}_{20})^I_1$	Σ^I_1	$(\overline{q}_{20})^I_2$	Σ^I_2
0	0.091	0.558	0.626	0.685	0.436	0.692	0.396	0.601	0.788	0.691	0.440	0.723
2	0.579	0.588	0.092	0.750	0.885	0.482	0.393	0.859	1.052	0.455	0.644	0.658
4	0.962	0.387	0.215	0.716	1.012	0.388	1.041	0.723	1.136	0.387	0.819	0.573
6	1.087	0.300	0.581	0.557	1.084	0.363	1.264	0.554	1.188	0.354	0.860	0.528
8	1.131	0.289	1.470	0.562	1.151	0.368	1.293	0.515	1.226	0.332	0.926	0.560

TABLE II. Spectroscopic quadrupole moments in e fm^2 for $I=2\hbar, 4\hbar, 6\hbar,$ and $8\hbar$ and $\sigma=1$ and 2 for the three nuclei considered in this paper.

	$\sigma=1$				$\sigma=2$			
	2	4	6	8	2	4	6	8
^{30}Mg	−13.79	−27.01	−32.43	−35.36	−3.11	−10.07	−21.48	−38.35
^{32}Mg	−19.15	−26.31	−30.09	−31.75	−8.63	−23.07	−27.22	−29.01
^{34}Mg	−20.78	−27.59	−31.27	−33.70	−15.16	−21.58	−25.34	−26.1

which gives us a measure of the average deformation of the underlying intrinsic states, and

$$(\overline{q^2_{20}})^I_\sigma = \int dq_{20} |g^I_\sigma(q_{20})|^2 q^2_{20} - [(\overline{q_{20}})^I_\sigma]^2, \qquad (8)$$

which serves as an estimation of the wave functions' spreading. The values of $(\overline{q_{20}})^I_\sigma$ and $\Sigma^I_\sigma = [(\overline{q^2_{20}})^I_\sigma]^{1/2}$ corresponding to the collective wave functions of Fig. 2 are given in Table I. We observe that the 0^+_1 and 2^+_2 states of ^{30}Mg are spherical (but with strong fluctuations in the q_{20} degree of freedom) whereas the 2^+_1 state is deformed ($\beta=0.25$). On the other hand, the 0^+_1 states of ^{32}Mg and ^{34}Mg are deformed with β values of 0.16 and 0.3, respectively and have a Σ^I_1 value rather high, possibly due to the small oblate hump. For spins higher than $I=0\hbar$ in ^{32,34}Mg and $I=4\hbar$ in ^{30}Mg the ground-state band is strongly deformed. The spreading of the wave functions gets smaller for increasing spins as expected. The excited bands also get more deformed for increasing spin, but their β values never coincide with that of the ground-state band. Obviously, their spreadings are bigger than for the ground-state band.

A more precise definition of the quadrupole moment for protons for each of the AMP-GCM states can be obtained from the results of the exact spectroscopic quadrupole moments $Q_\sigma(I)$ for protons (no effective charge has been used). The values obtained for each of the wave functions $|\Phi^I_\sigma\rangle$ are given in Table II for the three nuclei studied and $\sigma=1$ and 2. All the spectroscopic moments are negative indicating prolate intrinsic deformations.

We can also compute the total intrinsic quadrupole moments from the spectroscopic ones through the formula $(q^{int}_{20})^I_\sigma = -[(2I+3)/2I]Q_\sigma(I)A/Z$ where the $K=0$ restriction has been taken into account and also the fact that our q_{20} values are, by definition, a factor 0.5 smaller than Q_0. The factor A/Z is used to take into account the fact that the spectroscopic quadrupole moments are given in term of the proton mass distribution whereas the intrinsic quadrupole moments are the total ones. As can be readily observed from Table II the intrinsic quadrupole moments obtained from the spectroscopic ones agree rather well with the corresponding average $(\overline{q_{20}})^I_\sigma$ for low spins and deviate up to a 20% for spin $8\hbar$.

In Table III the energy splittings between different states and the $E2$ transition probabilities among them are compared with the available experimental data. Concerning the $B(E2,0^+_1 \to 2^+_1)$ transition probabilities we find a very good agreement with the only known experimental value and with the theoretical predictions of Utsumo *et al.* [23] using the Monte Carlo shell model (MCSM). The 2^+_1 excitation energies rather nicely follow the isotopic trend but they are larger than the experimental values by a factor of roughly 1.5. This discrepancy could be the result of using angular momentum projection after variation (PAV) instead of the more complete projection before variation (PBV) that will require for each value of the angular momentum the calculation of the generating states from the variational principle on the projected energy (see Sec. II). Usually, the PBV method yields to rotational bands with moments of inertia larger than the PAV ones [17,20].

A full PBV is, unfortunately, extremely costly to implement with large configuration spaces. Therefore, to estimate the effect of PBV in our results, we have resorted to the self-consistent cranking method which is an approximation to PBV in the limit of large deformations. We have chosen the intrinsic state with $q_{20}=1b$ as the most representative configuration (it approximately corresponds to the prolate minima in all the nuclei considered) and computed the projected energies. In addition, self-consistent cranking calculations with the constraints $q_{20}=1b$ in the quadrupole moment

TABLE III. Calculated and experimental results for excitation energies and $B(E2,0^+_{\sigma_1} \to 2^+_{\sigma_2})$ transition probabilities. In the experimental data columns values marked with an (*) correspond to Monte Carlo shell-model results taken from Ref. [23]. The experimental data for the excitation energies have been taken from [1] for the ^{32}Mg nucleus and from [25] for ^{30}Mg. The $B(E2)$ transition probability has been taken from [2].

	Calc. energies (MeV)			Expt.	Calc. $B(E2)e^2$ fm^4			Expt.
	$0^+_1-2^+_1$	$0^+_1-0^+_2$	$2^+_1-2^+_2$	$0^+_1-2^+_1$	$0^+_1\to2^+_1$	$0^+_1\to2^+_2$	$0^+_2\to2^+_2$	$0^+_1\to2^+_1$
^{30}Mg	2.15	2.30	1.60	1.482	229	3	218	300(*)
^{32}Mg	1.46	1.77	3.35	0.885	395	3.4	199	454±78
^{34}Mg	1.02	2.35	3.31	0.75(*)	525	0	290	580(*)

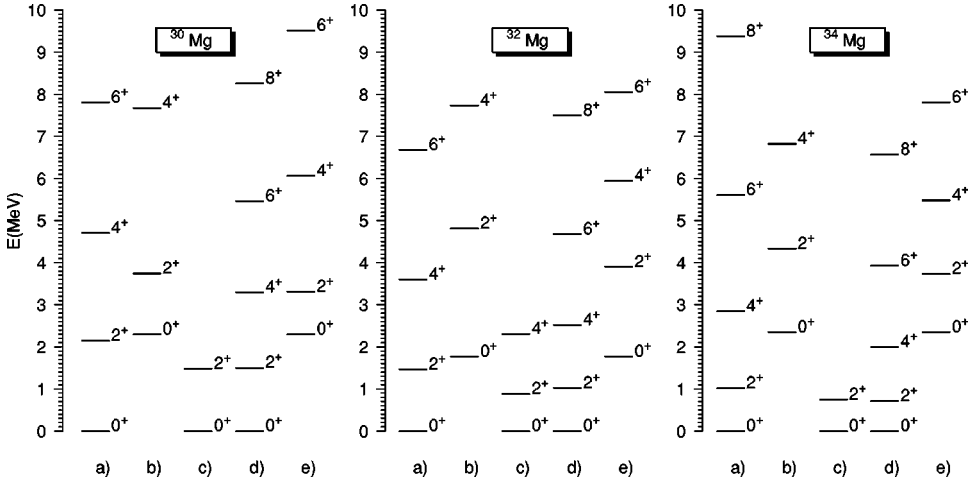

FIG. 3. Collective bands for the three nuclei studied. Bands (a) and (b) correspond to the AMP-GCM results for the ground and first excited band. (c) is the experimental band (in the case of ^{34}Mg the MCSM prediction of [23] has been used). Finally, bands (d) and (e) are the AMP-GCM results quenched by the factor 0.7 discussed in the text.

and $\langle J_x \rangle = \sqrt{I(I+1)}$ in the angular momentum have been performed. The cranking results for the excitation energies of the 2^+ state are 0.548, 0.591, and 0.571 MeV for ^{34}Mg, ^{32}Mg, and ^{30}Mg, respectively, whereas the corresponding projected quantities are 0.753, 0.873, and 0.895 MeV. The cranking excitation energies of the 2^+ state are a factor of 0.7 smaller than the projected ones and therefore, the effect of PBV is to increase the moment of inertia as compared to the PAV method. If we consider the reduction factor as significative (the q_{20} value chosen roughly corresponds to the position of the maxima of the collective wave functions) and apply it to our GCM results for the $0_1^+ - 2_1^+$ energy differences we obtain the values 0.71, 1.02 and 1.50 MeV for ^{34}Mg, ^{32}Mg, and ^{30}Mg, respectively. The new energy differences are in much better agreement with the experimental values and the MCSM results than the uncorrected ones. Also the corrected energy obtained for the 4_1^+ state of ^{32}Mg is in good agreement with the excitation energy of 2.3 MeV of a state of this nucleus which is a firm candidate to be the 4^+ state belonging to the yrast ''rotational band'' [24].

Although the previous estimation can be criticized in many ways we think it may serve as an indication that a full PBV will improve the results obtained here. Concerning the $B(E2)$ transition probabilities, the main effect of the PBV will be to shift down the $I=2\hbar, \ldots$ projected energy curves keeping its shape mostly unaffected. Therefore, we do not expect big changes both in the collective wave functions $g_\sigma^I(q_{20})$ and in the $B(E2)$ transition probabilities that depend on them.

Finally, the band energy diagrams for the three nuclei considered are shown in Fig. 3 for states with excitation energies smaller than 10 MeV. For each nuclei, the bands labeled (a) and (b) correspond to the AMP-GCM result for the yrast and excited bands, the band labeled (c) accounts for the experimental data in ^{30}Mg and ^{32}Mg and for the MCSM result in ^{34}Mg and finally, bands (d) and (e) stand for the GCM bands quenched by the factor of 0.7 previously discussed.

C. Results for other parametrizations of the Gogny force

The occurrence of quadrupole deformation in atomic nuclei is the result of the competition between two effects; namely, the surface energy which prevents deformation and the quantal shell effects which, depending on the nucleus, favor quadrupole deformation. It is therefore highly interesting to analyze the effect of these two aspects in the results we have obtained for the nucleus ^{32}Mg. To this end we have carried out calculations with two old parametrizations of the Gogny force; namely, the D1 and D1′ parametrizations [10]. The D1 parametrization was the one originally proposed by Gogny and the only difference with D1′ is the spin-orbit strength which is smaller for D1. As a result one can expect

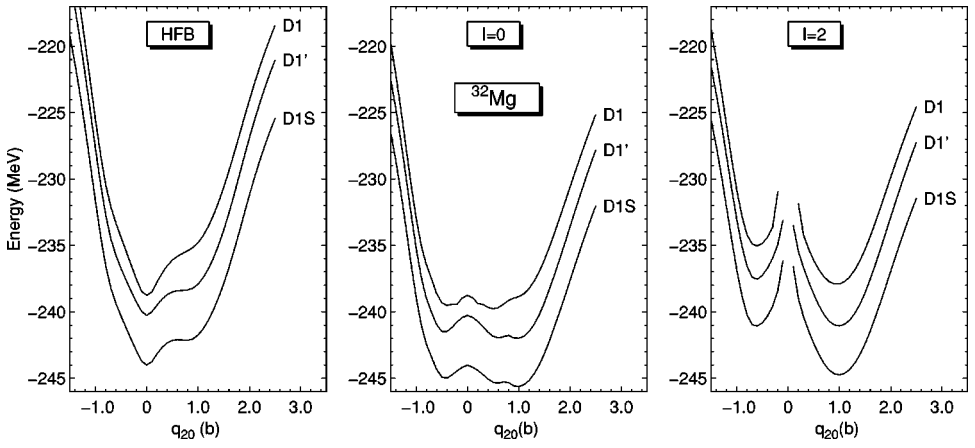

FIG. 4. HFB (right panel) and angular momentum-projected energy curves ($I=0\hbar$ middle panel, $I=2\hbar$ left panel) as a function of the mass quadrupole moment for the nucleus ^{32}Mg and the three parametrizations of the Gogny force considered.

TABLE IV. Results of the AMP-GCM calculations for ^{32}Mg and the parametrizations D1, D1′, and D1S of the Gogny interaction. The average quadrupole moments $(\overline{q}_{20})^I_\sigma$ for the ground-state band and spins 0 and 2 are given, in barns, in the first two columns. In the third column the $B(E2)$ transition probabilities in e^2 fm^4 are given. In the fourth column the excitation energy of the 2^+_1 state with respect to the ground state is given in MeV. Finally, in the last two columns the energy gaps $\Delta\epsilon_{f_{7/2}-d_{3/2}}$ and $\Delta\epsilon_{f_{7/2}-p_{3/2}}$ are given in MeV.

	$(\overline{q}_{20})^0_1$	$(\overline{q}_{20})^2_1$	$B(E2,0^+_1\rightarrow 2^+_1)$	$E_{0^+_1-2^+_1}$	$\Delta\epsilon_{f_{7/2}-d_{3/2}}$	$\Delta\epsilon_{f_{7/2}-p_{3/2}}$
D1	0.185	0.785	138	2.25	6.37	1.56
D1′	0.381	0.869	299	1.67	5.37	1.91
D1S	0.436	0.885	385	1.46	5.37	1.80

that D1 will lead to a higher $\Delta\epsilon_{f_{7/2}-d_{3/2}}=\epsilon_{f_{7/2}}-\epsilon_{d_{3/2}}$ energy gap than D1′ as it turns out to be the case: the value of $\Delta\epsilon_{f_{7/2}-d_{3/2}}$ is 6.37 MeV for D1 and 5.37 MeV for D1′. On the contrary, the value of $\Delta\epsilon_{f_{7/2}-p_{3/2}}$for D1 gets reduced from the 1.91 MeV we obtain for D1′ to the value 1.56 MeV. On the other hand, D1S has the same spin-orbit strength as D1′ (the values of $\Delta\epsilon_{f_{7/2}-d_{3/2}}$ and $\Delta\epsilon_{f_{7/2}-p_{3/2}}$ given in the previous paragraph for D1′ are very close to those of D1S given in a previous subsection) but its surface energy coefficient is smaller than in D1′. The need for a reduction of the surface energy coefficient in D1′ was evident when the fission barriers for ^{240}Pu [11] were computed with the Gogny force: they came out too high and the new D1S parametrization was proposed to cure this deficiency of the former D1′ parametrization.

In Fig. 4 we have plotted the HFB energy curves (left panel) and the AMP energies for $I=0\hbar$ (middle panel) and $I=2\hbar$ (right panel) for the three parametrizations of the Gogny force just mentioned. We observe that the results obtained for D1S and D1′ are, apart from the overall 4 MeV shift, very similar. This similarity is a clear indication that the value of the surface energy parameter has no influence on the results. The HFB result for D1 shows a shoulder at $q_{20}=1b$ which is located much higher in energy than the corresponding shoulder for D1S and D1′. As a consequence, the $I=0\hbar$ projected energy curve obtained with D1 shows a very shallow minimum at $q_{20}=0.5b$. However, the $I=2\hbar$ projected energy curves are very similar for the three parametrizations. The differences found between the D1 results and the ones with the two other parametrizations clearly indicate the sensitivity of the quadrupole properties of ^{32}Mg to the relative position of the orbits involved.

Finally, we have carried out the AMP-GCM calculation for the D1 and D1′ parametrizations of the force and the most important quantities obtained are summarized in Table IV. As expected from the projected energy curves of Fig. 4 we obtain a rather small average quadrupole moment $(\overline{q}_{20})^I_\sigma$ for $\sigma=1$ and $I=0\hbar$ with the D1 parametrization and bigger ones for the two other parametrizations. However, the $(\overline{q}_{20})^I_\sigma$ for $\sigma=1$ and $I=2\hbar$ are rather similar in the three cases. The smaller value of $(\overline{q}_{20})^0_1$ for the D1 parameters gets reflected in a much smaller $B(E2)$ transition probabilities than for the two other parametrizations. Finally, the excitation energy of the 2^+_1 state with respect to the ground state turns out to be significantly bigger for D1 than for the other parameter sets, being the results of D1′ and D1S in reasonable agreement. The final conclusion of this comparison is that the energy gap $\Delta\epsilon_{f_{7/2}-d_{3/2}}$ seems to be a relevant parameter in order to reproduce the properties of ^{32}Mg.

IV. CONCLUSIONS

In conclusion, we have performed angular momentum projected generator coordinate method calculations with the Gogny interaction D1S and the mass quadrupole moment as generating coordinate in order to describe rotational like states in the nuclei ^{30}Mg, ^{32}Mg, and ^{34}Mg. We obtain a very well deformed ground state in ^{34}Mg, a fairly deformed ground state in ^{32}Mg and a spherical ground state in ^{30}Mg. In the three nuclei, states with spins higher or equal $I=4\hbar$ are deformed. The intraband $B(E2)$ transition probabilities agree well with the available experimental data and results from shell-model-like calculations. The 2^+ excitation energies follow the isotopic trend but come out a factor of 1.5 too high as compared with the experiment. We attribute the discrepancy to the well-known deficiency of projection after variation calculations of providing small moments of inertia. However, we consider the agreement with experiment to be remarkable taking into account that the same force used in this calculation is also able to give reasonable values for such different quantities as fission barrier heights, moments of inertia of superdeformed bands, the energy of octupole vibrations, etc., in heavy nuclei. The sensitivity of the results to other parametrizations of the Gogny interaction is also analyzed and the conclusion is that the D1 parameter set fails to reproduce the properties of ^{32}Mg the spin-orbit strength being responsible for such failure.

Note added in proof. Upon completion of this work, new experimental results from RIKEN concerning the nucleus ^{34}Mg have become available [26]. The measured 2^+ and 4^+ excitation energies are 0.67 MeV and 2.13 MeV, respectively, and our predictions are in good agreement with them. We would like to thank Professor A. Poves for pointing out to us the results of Ref. [26].

ACKNOWLEDGMENTS

R.R.-G. kindly acknowledges the financial support received from the Spanish Instituto de Cooperacion Iberoamericana (ICI). This work has been supported in part by the DGICyT (Spain) under Project No. PB97/0023.

[1] D. Guillemaud-Mueller *et al.*, Nucl. Phys. **A426**, 37 (1984).
[2] T. Motobayashi *et al.*, Phys. Lett. B **346**, 9 (1995).
[3] A. Poves and J. Retamosa, Phys. Lett. B **184**, 311 (1987); Nucl. Phys. **A571**, 221 (1994).
[4] X. Campi, H. Flocard, A.K. Kerman, and S. Koonin, Nucl. Phys. **A251**, 193 (1975).
[5] M. Barranco and R.J. Lombard, Phys. Lett. **78B**, 542 (1978).
[6] R. Bengtsson, P. Moeller, J.R. Nix, and J. Zhang, Phys. Scr. **29**, 402 (1984).
[7] J. F. Berger *et al.*, Inst. Phys. Conf. Ser. **132**, 487 (1993).
[8] P.-G. Reinhard *et al.*, Phys. Rev. C **60**, 014316 (1999).
[9] R. Rodríguez-Guzmán, J.L. Egido, and L.M. Robledo, Phys. Lett. B **474**, 15 (2000).
[10] J. Dechargé and D. Gogny, Phys. Rev. C **21**, 1568 (1980).
[11] J.F. Berger, M. Girod, and D. Gogny, Nucl. Phys. **A428**, 23c (1984).
[12] P.-H. Heenen, P. Bonche, S. Cwiok, W. Nazarewicz, and A. Valor, nucl-th/9908083.
[13] L. M. Robledo, Phys. Rev. C **50**, 2874 (1994); J.L. Egido, L.M. Robledo, and Y. Sun, Nucl. Phys. **A560**, 253 (1993).
[14] R. G. Nazmitdinov, L.M. Robledo, P. Ring, and J.L. Egido, Nucl. Phys. **A596**, 53 (1996).
[15] K. Hara and Y. Sun, Int. J. Mod. Phys. E **4**, 637 (1995).
[16] P. Ring and P. Schuck, *The Nuclear Many-Body Problem* (Springer, Berlin, 1980).
[17] K. Hara, A. Hayashi, and P. Ring, Nucl. Phys. **A385**, 14 (1982).
[18] P. Bonche, J. Dobaczewski, H. Flocard, P.-H. Heenen, and J. Meyer, Nucl. Phys. **A510**, 466 (1990).
[19] A. Valor, J.L. Egido, and L.M. Robledo, Phys. Rev. C **53**, 172 (1996).
[20] K.W. Schmid and F. Grümmer, Rep. Prog. Phys. **50**, 731 (1987).
[21] F. Villars and N. Schmeing-Rogerson, Ann. Phys. (N.Y.) **63**, 433 (1971).
[22] W.A. Friedman and L. Wilets, Phys. Rev. C **2**, 892 (1970).
[23] Y. Utsumo, T. Otsuka, T. Mizusaki, and M. Honma, Phys. Rev. C **60**, 054315 (1999).
[24] F. Azaiez *et al.*, Proceedings of the International Conference ''Nuclear Structure 98,'' Gatlinburg, 1998.
[25] P.M. Endt, Nucl. Phys. **A521**, 1 (1990).
[26] K. Yoneda *et al.*, Proceedings of the International Conference RIB2000, Divonne, France (to be published).